11-23-2018

Chemical weathering across the western foreland of the Greenland Ice Sheet

Kelly M. Deuerling

Jonathan B. Martin

Ellen E. Martin

Jakob Abermann

Sille Marie Myreng

See next page for additional authors

Authors

Kelly M. Deuerling, Jonathan B. Martin, Ellen E. Martin, Jakob Abermann, Sille Marie Myreng, Dorthe Petersen, and Åsa K. Rennermalm

Chemical weathering across the western foreland of the Greenland Ice Sheet

Kelly M. Deuerling[a], Jonathan B. Martin[a], Ellen E. Martin[a], Jakob Abermann[bd], Sille Marie Myreng[b], Dorthe Petersen[b], Åsa K. Rennermalm[c]

A Department of Geological Sciences, University of Florida, Gainesville, FL 32611, USA

B Greenland Survey, Nuuk, Greenland

C Department of Geography, Rutgers University, Lucy Stone Hall, B214, 54 Joyce Kilmer Avenue, Piscataway, NJ 08854-8045, USA

D Department of Geography and Regional Science, University of Graz, Heinrichstraß 36, 8010 Graz, Austria

Abstract

Proglacial streams deliver melt water and chemical weathering products, including nutrients and radiogenic isotopes, from continental ice sheets to the ocean. Weathering products are also delivered to the ocean in non-glacial streams that form following ice sheet retreat and are disconnected from ice sheet meltwater by hydrologic divides. If weathering reactions differ in non-glacial and proglacial stream catchments, the streams could deliver different types and magnitudes of solutes to the ocean, depending on relative discharge volumes. Unlike proglacial streams, however, little is known of non-glacial stream solute compositions or discharge. Here we show specific discharges are similar from a proglacial stream draining the Greenland Ice Sheet (GrIS) with several streams disconnected from the ice sheet. We also evaluate weathering reactions across a 170-km transect in western Greenland that contains one proglacial stream draining the GrIS, and two coastal (ice distal) and three inland (ice proximal) areas with non-glacial streams. Non-glacial streams exhibit solute compositions and offsets between dissolved and bedload Sr isotope ratios that indicate weathering increases toward the coast with exposure age and precipitation. Major element mass balance calculations show weathering reactions shift from predominately carbonic acid weathering of carbonate minerals inland near the ice sheet to predominately sulfuric acid weathering of carbonate minerals near the coast. Strontium concentrations and isotopic ratios of the proglacial stream reflect mixing of at least two subglacial sources and minor in-stream weathering that consumes CO_2. About 5 times less CO_2 is consumed per liter in the proglacial than inland non-glacial streams; however, arid conditions inland suggest limited discharge from the ungauged inland streams leads to less total CO_2 weathering than proglacial stream. One coastal area consumes less CO_2 per liter than the proglacial stream and another coastal area exhibits net CO_2 production. These results indicate estimates for glacial foreland solute fluxes and CO_2 weathering consumption and production should include estimates from both non-glacial and proglacial streams. Understanding weathering fluxes from these two types of

streams will be important for evaluations of past ice sheet retreat and predictions of future solute and CO_2 fluxes associated with continued ice sheet retreat.

Keywords

Greenland Ice Sheet, Chemical weathering, Glacial retreat, CO_2, Radiogenic isotopes, Watersheds

1. Introduction

Since the Last Glacial Maximum (LGM) about 18 thousand years before present (ka), Northern Hemisphere continental ice sheets have retreated and exposed vast high-latitude landscapes (Dyke and Prest, 1987, Stroeven et al., 2016). These landscapes are underlain by bedrock, poorly sorted glacial debris, and abundant fine-grained and chemically reactive comminuted sediment. Weathering of these reactive sediments during ice sheet retreat may have altered seawater composition, as suggested by large nutrient fluxes from modern proglacial streams draining meltwater from the Greenland Ice Sheet (GrIS) (e.g., Bhatia et al., 2010, Hawkings et al., 2014, Hawkings et al., 2015, Hawkings et al., 2016, Meire et al., 2016, Hawkings et al., 2017). Meltwater discharged from proglacial streams in both hemispheres during the last deglaciation led to ~130 m of sea level rise (e.g., Lambeck et al., 2002, Miller et al., 2005). Within the glacial foreland, streams also drain watersheds on newly exposed landscapes that are disconnected from the ice sheet by hydrologic divides (herein referred to as "deglaciated watersheds" that drain "non-glacial streams"). Non-glacial streams have no effect on sea level as they discharge only precipitation, groundwater, and permafrost meltwater. However, we hypothesize that non-glacial stream compositions, and thus their oceanic fluxes, may differ from proglacial streams, and therefore oceanic fluxes from glacial forelands should vary in predictable ways as ice sheets retreat.
Variations in weathering inputs to the ocean during the last deglaciation are reflected in increasing seawater Pb isotope ratios recorded in deep-sea sediments (Foster and Vance, 2006, Kurzweil et al., 2010, Crocket et al., 2012). This increase is attributed to rapid weathering of freshly exposed glacial material and changes in reaction products as the extent or "maturity" of weathering increased. Here, weathering maturity reflects either (1) the magnitude of incongruent weathering of mineral phases, such as biotite, monazite, sphene and allenite, that are enriched in parent radioisotopes (e.g., ^{87}Rb, $^{235,238}U$, and ^{232}Th), or (2) the quantity of radiogenic isotopes extracted from lattice sites damaged by radioactive decay. Weathering maturity increases with exposure age of soil chronosequences associated with mountain glacier retreat (Erel et al., 1994, White et al., 1996, Blum and Erel, 1997, Harlavan et al., 1998, Harlavan and Erel, 2002, Harlavan et al., 2009) and could control the observed increase in seawater Pb isotope ratios (Foster and Vance, 2006, Kurzweil et al., 2010, Crocket et al., 2012). In western Greenland, the site of this study, weathering maturity in deglaciated watersheds increases with both increased exposure age and precipitation (Scribner et al., 2015).

The proglacial and deglaciated watersheds in western Greenland provide an ideal setting to study chemical weathering during ice sheet retreat. Similar condensed exposures of the glacial foreland are not available over most of the northern high latitudes because of retreat of the large ice sheets since the LGM (Dyke and Prest, 1987, Stroeven et al., 2016). Proglacial streams draining the GrIS are widely studied to evaluate potential effects on sea level rise (Mernild et al., 2010, Bamber, 2012, Rennermalm et al., 2012, van As et al., 2017, Bamber et al., 2018) and to assess solute fluxes to the ocean, including major elements (Yde et al., 2005, Yde et al., 2014), Fe (Bhatia et al., 2013b), DOC (Bhatia et al., 2013a), macronutrients, including silica, nitrogen and phosphorous (Hawkings et al., 2014, Hawkings et al., 2015, Hawkings et al., 2016, Meire et al., 2016, Hawkings et al., 2017), and atmospheric exchange of CO_2 (Ryu and Jacobson, 2012). However, little is known about weathering and solute fluxes from non-glacial streams (e.g., see Wimpenny et al., 2010, Wimpenny et al., 2011, Scribner et al., 2015) and no systematic comparison exists of proglacial and non-glacial stream compositions across western Greenland such as we present here. Proglacial and non-glacial stream compositions should differ because of their distinct sources of water. Proglacial streams discharge water from (1) supraglacial runoff, (2) subglacial watersheds that include basal meltwater and surface meltwater captured by moulins (Anderson et al., 1997, Anderson et al., 2000, Andrews et al., 2014), and (3) non-glacial tributaries. The sub- and supra-glacial environments provide many of the proglacial stream solutes (Hawkings et al., 2016) and may change downstream in response to delivery from tributaries and in situ reactions (e.g., Ryu and Jacobson, 2012) particularly in outwash plains (sandurs) (Deuerling et al., 2018). Rapid melting can generate high flow rates that dilute solute concentrations and elevate turbidity. In contrast, non-glacial streams, which are sourced predominately from runoff and groundwater, have lower suspended sediment loads and higher average solute concentrations than proglacial streams (Wimpenny et al., 2010, Wimpenny et al., 2011). Compositions of the solute loads change with weathering maturity within deglaciated watersheds (Scribner et al., 2015).

In addition to limited information on differences between proglacial and non-glacial stream compositions, data on solute fluxes are limited because they require discharge measurements that are rare for non-glacial streams (Abermann et al., 2018) but somewhat better constrained for proglacial streams due to concerns about their impact on sea level (e.g., Mernild et al., 2009, Mernild et al., 2010, Rennermalm et al., 2012, van As et al., 2017). Relative differences in global discharge from proglacial and non-glacial streams through time will depend on extents of ice-free versus ice-covered areas, precipitation patterns across glacial forelands, and rates of ice sheet melting; however, non-glacial stream discharge should increase relative to proglacial discharge as ice-free landscapes increase during glacial terminations. A shift from predominately proglacial to non-glacial discharge should thus affect oceanic solute fluxes depending on watershed weathering maturity and resulting stream compositions.

To evaluate potential differences in proglacial and non-glacial stream solute fluxes, we compare available discharge data from a proglacial stream and several streams draining watersheds disconnected from the GrIS, some of which contain mountain glaciers and small ice caps. We also compare stream compositions from five deglaciated areas containing multiple non-glacial streams and one proglacial stream in

western Greenland (Fig. 1), using a mass balance approach (Galy and France-Lanord, 1999, Spence and Telmer, 2005, Ryu and Jacobson, 2012). The mass balance separates carbonic and sulfuric acid weathering of carbonate and silicate minerals and estimates mass exchange of CO_2. We use Sr isotope ratios to evaluate shifts in potential weathering contributions of radiogenic isotopes to the ocean. These data and models suggest proglacial and non-glacial streams have distinct contributions to ocean and atmospheric chemistry.

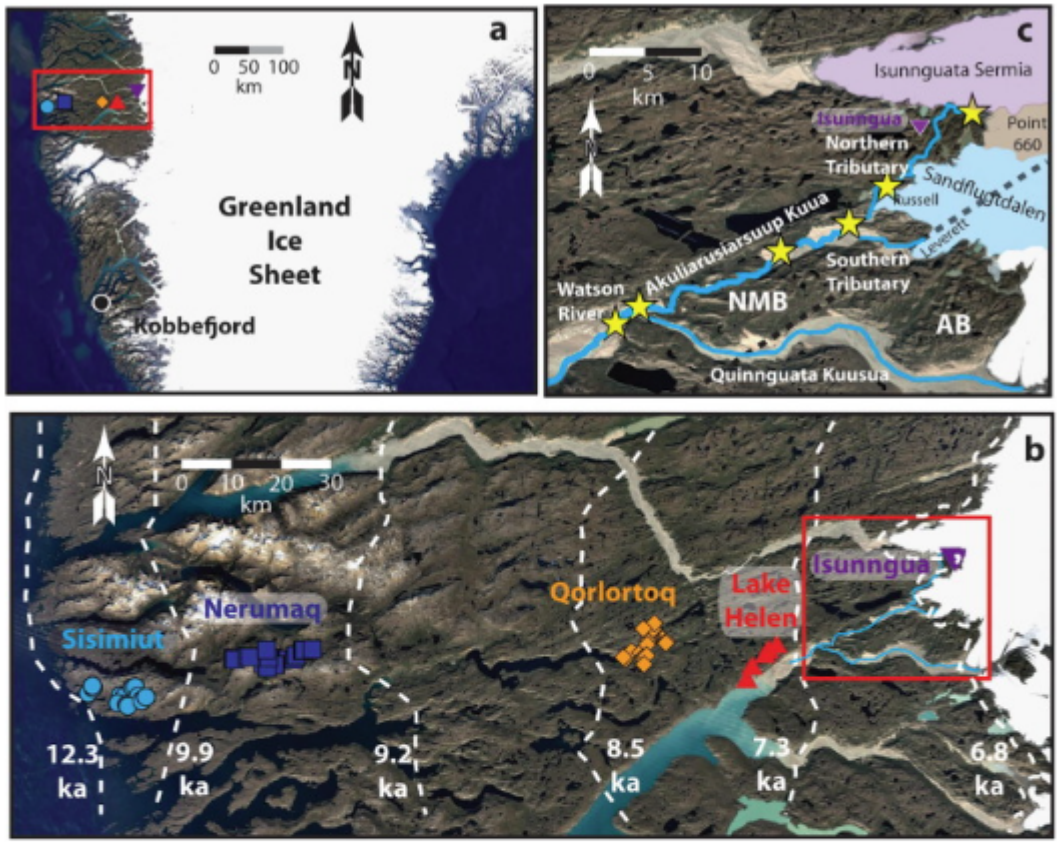

Download : Download high-res image (595KB) Download : Download full-size image

Fig. 1. Annotated Google Earth images illustrating the field location. (a) Central Greenland showing sample transect and Kobbefjord locations. Red box shows outline for panel b. (b) Individual sample locations from sampled deglaciated areas: Sisimiut (light blue circles), Nerumaq (dark blue squares), Qorlortoq (orange diamonds), Lake Helen (red point-up triangles), and Isunngua (purple point-down triangles). Moraine ages (white dashed lines) are from Levy et al. (2012). Red box shows outline for panel c. (c) Area surrounding Watson River/Akuliarusiarsuup Kuaa/Quinnguata Kuusua watershed illustrating sample locations in the proglacial system (yellow stars), subglacial drainage basins boundaries and names (purple shading – Isunnguata Sermia; brown shading – Point 660; light blue shading – Sandflugtdalen) proposed by Lindbäck et al. (2015). River names used in the paper are shown. The black dotted line shows the approximate NMB-AB lithologic boundary from Dawes (2009).

2. Setting – Western Greenland geology, climate, and hydrology

The GrIS has retreated approximately 170 km from the coast of western Greenland over the past ~12 ky and exposed the Proterozoic orthogneiss of the Nagssugtoqidian Mobile Belt (NMB) (Fig. 1, Levy et al., 2012). The NMB underlies all of the deglaciated watersheds sampled for this project (Pedersen et al., 2013) and because of its relatively homogeneous composition, solute variations between non-glacial streams should result from differences in weathering maturity (Scribner et al., 2015). The NMB is bordered on the south by quartzo-feldspathic gneisses of the Archean Block (AB) (Dawes, 2009) and these two units have distinct Pb, Sr, and Nd isotope ratios (Colville et al., 2011, Reyes et al., 2014). The NMB-AB contact extends northeast for tens of kilometers beneath the ice sheet near the terminus of the Leverett Glacier (van Gool et al., 2002, Stendal and Garde, 2005, Dawes, 2009) and crosses Isunnguata Sermia, Sandflugtdalen and Point 660 subglacial drainage basin in the region (Fig. 1, Lindbäck et al., 2015). Water discharging from these drainages could thus have distinct isotopic compositions, reflecting differences in NMB or AB isotopic compositions.

Retreat of the GrIS formed many deglaciated watersheds between the current ice edge and the coast that have increasing exposure ages with distance from the ice (Fig. 1b). Moraine ages range from ~10 ka at the coast to ~7 ka near the GrIS, with <0.2 ka Little Ice Age moraines adjacent to the GrIS (Levy et al., 2012). The current position of the ice sheet affects the regional climate, which is arid near the ice sheet with annual precipitation at Kangerlussuaq averaging around 150 mm/yr, while a maritime influence results in precipitation at Sisimiut of 300 to 400 mm/yr (Hasholt and Sogaard, 1978, Anderson et al., 2001, Cappelen, 2018).

Literature references to proglacial streams in the study area include both English and Greenlandic names, which has led to some confusion of locations. In this paper we refer to the Watson River as the proglacial stream that extends from the confluence of two major proglacial rivers in the region, the Akuliarusiarsuup Kuua (AKR) and Quinnguata Kuusua rivers, to Kangerlussuaq Fjord (Danish: Søndre Strømfjord; Fig. 1). The AKR headwaters consist of two unnamed tributaries. The southern tributary originates as sub-glacial and supraglacial discharge from the Leverett Glacier and flows ~ 5 km to its confluence with the northern tributary (e.g., Hindshaw et al., 2014). The northern tributary is approximately 15 km long and originates as sub-glacial and supraglacial discharge from the Isunnguata Sermia glacier. This tributary flows ~8 km across deglaciated terrain that we refer to here as Isunngua based on the Greenlandic name for the region between Isunnguata and Russell glaciers (Fig. 1c). The northern tributary then flows in front of the Russell Glacier for about 5 km where it gains more sub- and supra-glacial water and across approximately 3-km of sandurs to its confluence with the southern tributary. Herein, we refer to this overall stream complex as the “AKR/WR”.

Long-term discharge records are rare for Greenlandic streams and are unavailable for the non-glacial streams between the ice edge near Kangerlussuaq and the coast near Sisimiut that were sampled for this project. Single measurements of multiple watersheds in the region during summer 1977 (Hasholt and Sogaard, 1978) show smaller specific discharge from streams near the GrIS (<1 L/sec/km^2) than from coastal non-glacial streams (maximum 22 L/sec/km^2), reflecting the precipitation gradient. Long-term measurements of non-glacial streams are available from four watersheds disconnected from the GrIS located ~300 km south of our field area and one ~10 km north of our field area, all of which contain small ice caps or mountain glaciers. The long-term records

from the non-glacial streams and AKR/WR (Electronic Access) indicate specific discharges are similar within a factor of 2 to 3 (Table 1). This similarity suggests that solute fluxes from these two types of streams may depend more on concentrations derived from weathering than discharge.

Table 1. Comparison of specific discharge (all values are $\times 10^6$ $m^3/yr/km^2$).[a]

Water year[b]	Proglacial					Disconnected from ice sheet					
Catchment and size (km^2)	Watson			AK004		650	654	655	656	Pisissarfik	
	6927[c]	9743[d]	12,547[e]	36	64	32.15	9.97	18.21	6.57	39	
2008	0.8	0.6	0.4	1.7[f]	3.1[f]	1.4	0.9	1.3		WY[h]	D[h]
2009	0.7	0.5	0.4	1.6	2.9	0.9	0.7	1.1	1.1	1997	0.5
2010	1.6	1.1	0.9	2.0	3.5	0.8	1.0	1.2	1.2	1998	0.4
2011	1.1	0.8	0.6	1.3	2.4	0.9	0.7	1.1	1.2	1999	0.3
2012	1.5	1.1	0.9	1.7	3.1	1.8	1.4	1.9	2.1	2000	0.5
2013	0.6	0.4	0.3	0.8[g]	1.5[g]	1.2	1.2	1.6	1.7		
2014	1.0	0.7	0.5			1.2	1.1	1.6	1.7		
2015	0.5	0.4	0.3				1.0	1.5	1.6		

a Data for Watson River obtained from van As et al. (2017); for AK004 from Rennermalm et al. (2014) and for the Kobbefjord streams from the ClimateBasis programme within the Greenland Ecosystem Monitoring Programme (www.g-e-m.dk).

b Water year calculated from Feb. 1 through Jan. 31.

c Watershed area from Mernild and Hasholt (2009).

d Watershed area from Fitzpatrick et al. (2014).

e Watershed area from van As et al. (2012).

f Data from June 8, 2008 through Jan. 31, 2009.

g Data from Feb. 1, 2013 through Aug. 13, 2013.

h WY – water year; D – discharge.

3. Methods

3.1. Sampling locations and collection

Chemical data reported here are based on samples that were collected from the proglacial AKR/WR watershed in western Greenland and five deglaciated areas between Kangerlussuaq to Sisimiut that contain multiple separate watersheds (Fig. 1). Data from four of the deglaciated areas, Sisimiut, Nerumaq, Qorlortoq, and Lake Helen, were reported previously in Scribner et al. (2015), who divided them into coastal (Sisimiut and Nerumaq) and inland (Qorlortoq and Lake Helen) watersheds based on geochemical differences. New data reported here include two non-glacial streams that drain into the AKR northern tributary and the AKR/WR proglacial stream. (All data presented here are provided in the Electronic Annex and are archived at the Arctic Data Center (Martin et al., 2018)). The ice-proximal non-glacial streams are separated from each other and the ice sheet by hydrologic divides and are collectively referred to as Isunngua because of similar exposure ages and annual precipitation. Similarly, two of the four areas previously described in Scribner et al. (2015) contain multiple watersheds. Two separate watersheds drain to a fjord in the Sisimiut area and to a lake in the Qorlortoq area. Nerumaq and Lake Helen watersheds consist of several nested watersheds that drain through a single non-glacial stream to fjords. Additional new data include three samples collected from AKR northern tributary (no samples were collected from the southern tributary), two samples from the main AKR channel and one sample from the Watson River (Fig. 1c).

Samples were collected between June 5 and July 23, 2013 (Table 2), after most snow had melted from the deglaciated watersheds. Although we recognize that water compositions evolve throughout the melt season (e.g., Hindshaw et al., 2014), the time required to move between sampling sites and to access sites within the areas prevented time-series collection of water. Nonetheless, this sampling scheme addressed our primary goal of evaluating spatial variations in water and sediment chemistry across age and precipitation gradients and between non-glacial and proglacial streams. Within our sampling window (e.g., after the peak of the melt season), proglacial water chemistry could vary daily as a result of diurnal variations in melting and freezing on the GrIS. The time to collect each sample was <1 hr and travel between the AKR/Watson sampling sites was 1–2 h, which was sufficient time for us to collect all samples at a similar point on the hydrograph over a period of two days (Table 2), assuming a residence time of water in the stream channel of around 10 h (Hasholt et al., 2013).

Table 2. Watershed sampling dates and number of samples (n).

Watershed	Sample date (2013)	n
Isunngua	June 5 to June 8	7
Lake Helen	June 9 to June 12	5
Sisimuit	June 18 to June 23	17
Nerumaq	June 26 to July 3	22
AKR/WR	July 8 to July 9	6
Qorlortoq	July 19 to July 23	19

Samples were collected by pumping water from near the center of the channel at a rate of around 1 L/min using a peristaltic pump fitted with Tygon tubing. The tubing led to an overflow cup in which a YSI ProPlus sonde was installed. The sonde, which was calibrated daily, was used to monitor temperature (T), specific conductivity (SpC; electrical conductivity normalized to 25 °C), pH, and dissolved oxygen (DO) concentration and saturation. These parameters were monitored until stable, after which the tubing was fitted with a 0.45 μm high-capacity trace metal grade canister filter and water was collected in various types of sample bottles specific for each analyte. The bottles and caps were rinsed three times with filtered sample water prior to filling. Cation samples were collected in 20 mL HDPE bottles and Sr isotope samples were collected in 0.25 to 1 L HDPE bottles. These bottles were prewashed in 10% trace metal grade HNO_3 and samples were preserved with Optima grade HNO_3 to pH < 2. Anion samples were collected in 20 mL DI-washed HDPE bottles with no preservative. Dissolved inorganic carbon (DIC) samples were collected in 20 mL Qorpac glass bottles by filling the bottles from the bottom, allowing water to overflow the bottle rim, and then closing the bottles while ensuring no bubbles were present. The water was poisoned with a saturated solution of mercuric chloride to eliminate subsequent microbial processes that may alter DIC concentrations. Nitrile or vinyl gloves were worn at all times to minimize contamination.
Bedload samples were collected in new Whirl-Pak bags using either a plastic trowel or gloved hand. Large samples were collected in an attempt to maintain particle size distribution. Samples were stored at 4 °C and shipped to the University of Florida. Suspended sediment was collected from proglacial streams by initially settling 1 L of unfiltered sample water, then decanting ~800 ml and evaporating the remaining water. All solid samples were stored refrigerated in the laboratory until aliquots were dried in a 60 °C oven.

3.2. Sample analyses

Major element concentrations were measured on a Dionex ICS-1600 (cations) and ICS-2100 (anions) ion chromatograph. Calibration curves were determined with custom multi-element standards, and repeated analyses of a diluted Dionex multi-element standard. Duplicate samples replicated within 5%. Alkalinity of the non-glacial stream water was measured in the field laboratories within 24 h of collection by titration with 0.1 N HCl using the Gran method. Duplicate analyses reproduced to <5%. Because of difficulty of measuring alkalinity in dilute samples of proglacial streams, alkalinity of the AKR/WR samples was calculated based on the DIC concentrations and pH measurements; we assume the calculated alkalinity is carbonate alkalinity. DIC samples were analyzed on an AutoMate Prep Device coupled to a UIC (Coulometrics) 5011 carbon coulometer. Repeated analyses of a 24.0 μg C standard replicated within 1%. Silica concentrations were measured within 30 days of collection on a Hach DR/890 portable spectrophotometer using a Heteropoly Blue method optimized for low SiO_2 concentrations (<1.6 mg/L) with a precision of around 10% based on repeated measurements of an in-house standard. Charge balance errors are typically ≤5%, although higher (at most ~15%) for the dilute water collected from AKR/WR.

Strontium isotope ratios were measured on aliquots of stream waters calculated to contain ~100 ng of Sr. These aliquots were evaporated to dryness in clean Teflon beakers, then dissolved in concentrated Optima HNO_3 to oxidize organic matter and dried. The residue was dissolved in 3.5 N HNO_3 and passed through Sr Spec resin to separate Sr, which was loaded onto degassed tungsten filaments. Ratios of $^{87}Sr/^{86}Sr$ were measured with a Micromass Sector 54 thermal ionization mass spectrometer (TIMS) in dynamic mode. Two hundred ratios were collected at 1.5 V ^{88}Sr and corrected for mass bias using $^{86}Sr/^{88}Sr = 0.1194$. Long-term analyses of NBS-987 in the University of Florida laboratory yields an $^{87}Sr/^{86}Sr$ value of 0.71025 +/− 0.00002, 2σ. Procedural blanks of 100 pg Sr were at least three orders of magnitude smaller than sample abundances

Strontium isotope ratios were also measured on bedload (<2 mm fraction) and suspended sediments. Approximately 3 g of the sieved bedload sample was crushed and combusted at 450 °C for 4 h to burn off organic matter. Approximately 0.05 g of both crushed bedload and suspended sediment was dissolved in a mixture of concentrated HF and HNO_3, and evaporated to dryness. Fluorides were then converted to chlorides in 6 N HCl and the sample was dried down for isotopic analysis. Sr was isolated using a two-step procedure with a primary column packed with BioRad AG 50W-X12 cation resin followed by Sr Spec column chemistry. Isotope ratios were measured using wet plasma on a Nu Plasma multi-collector inductively coupled plasma mass spectrometer (MC-ICPMS) and a time resolved analysis (TRA) technique (Kamenov et al., 2008). $^{87}Sr/^{86}Sr$ was corrected for mass bias using $^{86}Sr/^{88}Sr = 0.1194$ and ^{87}Sr was corrected for interference of ^{87}Rb by monitoring ^{85}Rb. The average $^{87}Sr/^{86}Sr$ of TRA measurements of NBS 987 = 0.71025 ± 0.00003, 2σ. Procedural blanks of 250 pg Sr were at least seven orders of magnitude smaller than sample abundances.

3.3. Mass balance and mixing models

Modified mass balance calculations (Galy and France-Lanord, 1999, Spence and Telmer, 2005, Ryu and Jacobson, 2012) were used to evaluate weathering mechanisms (Electronic Annex). Briefly, the major solute concentrations were apportioned to one of four specific weathering mechanisms utilizing the stoichiometry of carbonate and silicate mineral weathering reactions by H_2CO_3 or H_2SO_4 after accounting for marine aerosol deposition (Table 3). We assume H_2CO_3 originates from hydration of CO_2, derived either from dissolution of atmospheric CO_2 or from remineralization of organic carbon. The stoichiometries of weathering reactions (Table 3) were then used to estimate the mass of CO_2 consumed or produced.

Table 3. Stoichiometry of weathering reactions.

Carbonic Acid	**Carbonate weathering – CO_2 sink**	
	$(Ca, Mg)CO_3 + CO_2 + H_2O \leftrightarrow (Ca^{2+}, Mg^{2+}) + 2HCO_3^-$	(1)
	Silicate weathering – CO_2 sink	
	$(Na, K)AlSi_3O_8 + CO_2 + 5.5H_2O \leftrightarrow (Na^+, K^+) + HCO_3^- + 0.5Al_2Si_2O_5(OH)_4 + 2H_4SiO_4$	(2)
	$(Ca, Mg)Al_2Si_2O_8 + 2CO_2 + 3H_2O \leftrightarrow (Ca^{2+}, Mg^{2+}) + 2HCO_3^- + Al_2Si_2O_5(OH)_4$	(3)
Sulfuric Acid	**Carbonate weathering – CO_2 source**	
	$2(Ca, Mg)CO_3 + H_2SO_4 \leftrightarrow 2(Ca^{2+}, Mg^{2+}) + SO_4^{2-} + H_2O + CO_2$	(4)
	Silicate weathering – CO_2 neutral	
	$2(Na, K)AlSi_3O_8 + H_2SO_4 + 9H_2O \leftrightarrow 2(Na^+, K^+) + SO_4^{2-} + Al_2Si_2O_5(OH)_4 + 4H_4SiO_4$	(5)
	$(Ca, Mg)Al_2Si_2O_8 + H_2SO_4 + H_2O \leftrightarrow (Ca^{2+}, Mg^{2+}) + SO_4^{2-} + Al_2Si_2O_5(OH)_4$	(6)

Two end-member mixing of solute sources to the AKR northern tributary was modeled based on $^{87}Sr/^{86}Sr^*$ and Sr* concentrations (Faure, 1986), assuming two potential sources, one from the NMB and the other from the AB (Electronic Annex). Distinct $^{87}Sr/^{86}Sr$ ratios of these two lithologies (Colville et al., 2011, Reyes et al., 2014) provide a useful tracer for mixing. End-member values for the mixing model are taken from Hindshaw et al., (2014) for the Leverett Glacier and from measurements made for this study for the Isunnguata Glacier (Table 4).

Table 4. Mixing endmember compositions.

Location	Date Sampled	Sr*[a] (μM)	$^{87}Sr/^{86}Sr^*$[1]
Southern Tributary[b]	June 5, 2009	76	0.745
Southern Tributary[b]	August 1, 2009	58	0.741
Northern Tributary	July 9, 2013	17	0.724

a

Asterisk (*) indicates corrected for marine aerosols.

b

Data from Hindshaw et al. (2014).

4. Results

4.1. Solute concentration variations

Specific conductivities in the non-glacial streams range from 31 to nearly 1632 µS/cm (Fig. 2a). These values are three times to nearly two orders of magnitude greater than the proglacial stream, which has values ranging from 6 to 16 µS/cm. These values increase from the headwaters near Isunnguata Glacier to the sample collected ~4 km downstream of the confluence of the northern and southern tributaries. The SpC remains around 16 µS/cm downstream of this point.

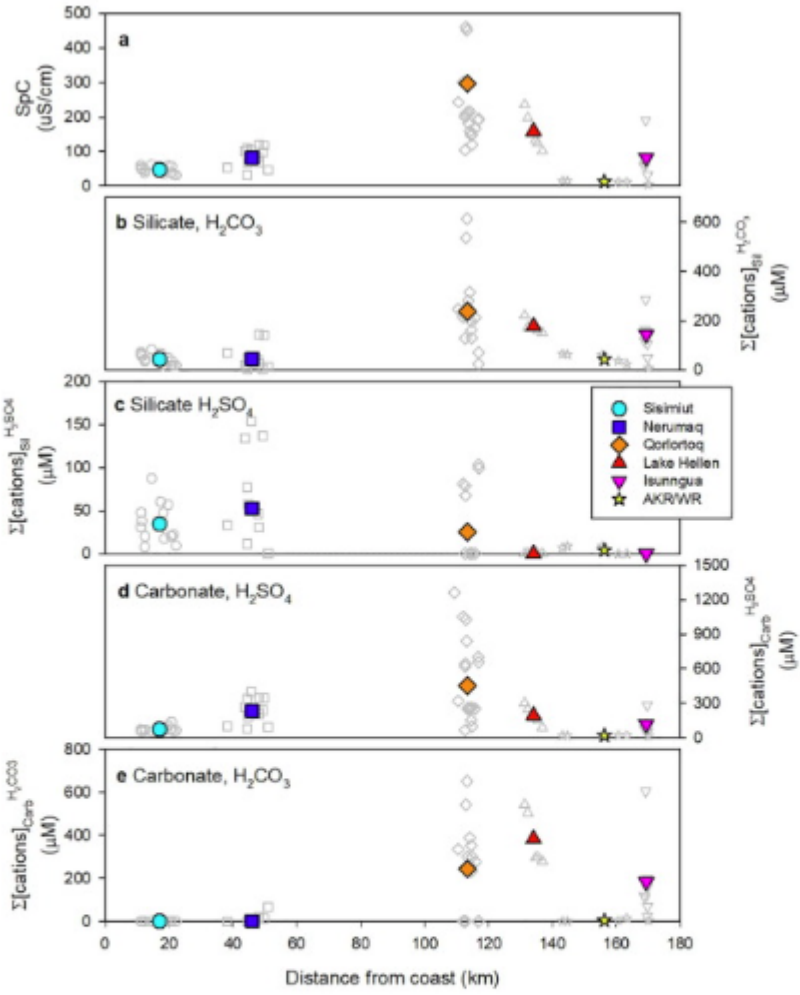

Download : Download high-res image (186KB) Download : Download full-size image

Fig. 2. Trends of specific conductivity and cation concentrations on a per liter basis (µmol/l) derived from mineral weathering versus distance from coast across the GrIS foreland. (a) Specific conductivity. (b) H_2CO_3 weathering of silicates, (c) H_2SO_4 weathering of silicates, (d) H_2SO_4 weathering of carbonates, and (e) H_2CO_3 weathering of carbonates. Note variations in scale on the Y axis. Open symbols are individual samples and filled symbols are average values for each watershed. (For interpretation of colour in this figure, the reader is referred to the web version of this article.)

In addition to differences in bulk concentration shown by specific conductivity, the relative solute compositions change between non-glacial and proglacial streams, as well as between the inland and coastal deglaciated watersheds. Specifically, the relative proportions of Si, Na + K, SO4, and HCO3 + CO3 are greater in the coastal than inland non-glacial streams (Fig. 3). These differences were qualitatively interpreted by Scribner et al. (2015) to reflect an increase in weathering maturity as a function of exposure age and precipitation in the Nerumaq and Sisimiut watersheds compared to Lake Helen and Qorlortoq watersheds, given the uniform NMB bedrock composition across the deglaciated drainages. We attempt to verify this qualitative interpretation through estimates of weathering maturity based on our mass balance model.

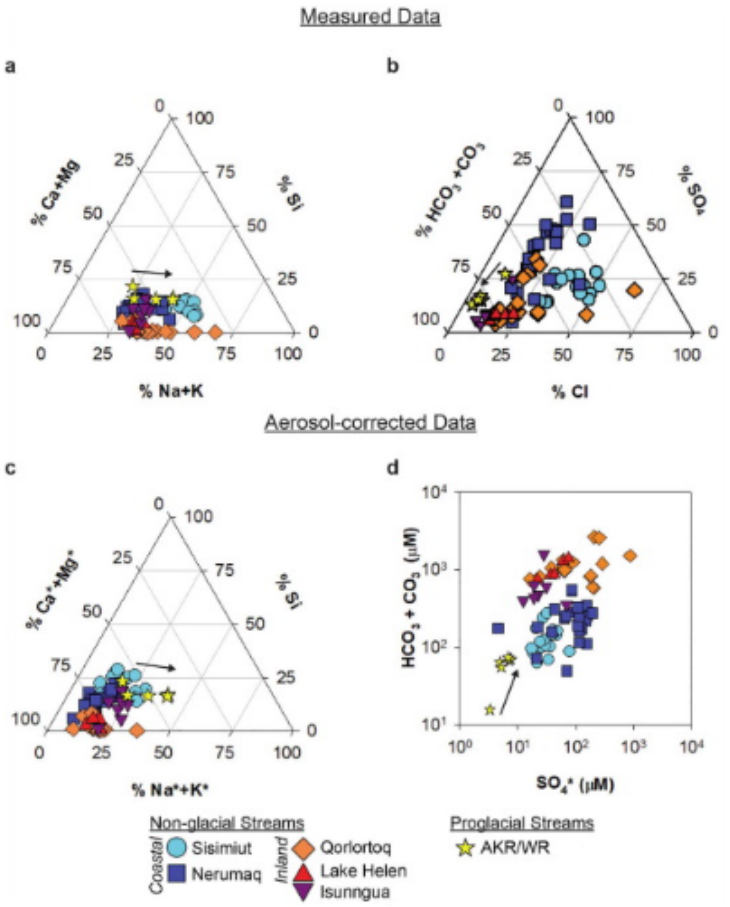

Download : Download high-res image (261KB) Download : Download full-size image

Fig. 3. Ternary diagrams of relative concentrations (micromolar) of major ions in all watersheds including aerosols (a-b) and aerosol-corrected (c) relative concentration based on the assumption that Cl originates only from marine solutes. (d) Cross plot of SO_4 and ($H_2CO_3 + CO_3$) concentrations on a Cl-free basis. Sisimiut, Nerumaq, Qorlortoq, and Lake Helen data are from Scribner et al. (2015). The data show elevated Ca, Mg, and $HCO_3 + CO_3$ concentrations in inland non-glacial streams and downstream in the AKR/WR relative to the coastal streams and upstream in the Watson River. Arrows indicate downstream direction of AKR/WR samples. (For interpretation colour in this figure, the reader is referred to the web version of this article.)

4.2. Weathering mass balances

Our mass balance calculations shows individual samples within all deglaciated watersheds have variable amounts of carbonate and silicate mineral weathering by H_2CO_3 and H_2SO_4 on a per liter basis (Fig. 2). The H_2SO_4 weathering of silicates contributes less solutes than the other three solute sources with the greatest contributions occurring in the two coastal watersheds (Sisimiut, Nerumaq), and also the inland watershed that is farthest from the ice sheet (Qorlortoq). Solute contributions from the other three weathering mechanisms show a larger range for all samples in the inland watersheds (Qorlortoq, Lake Helen, and Isunngua) than the coastal watersheds (Sisimiut and Nerumaq).

We have found little systematic downstream variations in compositions within individual non-glacial streams. We evaluated differences of the watershed means used Student's t-test and found the differences were statistically significant at $p < 0.05$. Therefore, the following analyses focuses on average solute compositions of each watershed, which exhibit consistent trends from the ice sheet to near the coast. Specifically, solutes derived from H_2CO_3 weathering of silicates and carbonates are elevated in the inland watersheds by several hundred μM compared with those solutes in the coastal watersheds (Fig. 2b and e). In contrast, average H_2SO_4 weathering of silicate minerals is slightly lower (~20 to 40 μM) in inland than coastal watersheds (Fig. 2c). The H_2SO_4 weathering of carbonate minerals is similar across the transect, but on average increases slightly from watersheds near the ice edge to Qorlortoq and then decreases to the coastal watersheds (Fig. 2d). The AKR/WR samples exhibit mostly H_2CO_3 and H_2SO_4 weathering of silicate minerals that increase downstream (Fig. 2b and c). However, the overall per liter mass of weathering products is one to two orders of magnitude smaller in AKR/WR compared to deglaciated watersheds because of dilute solute concentrations, as reflected in the low specific conductivities (Fig. 2a).

To alleviate complications in comparisons of weathering magnitudes caused by variations in solute concentrations as reflected in specific conductivities (Fig. 2a), we evaluate relative contributions from each weathering mechanism across the transect (Fig. 4). Most solutes in inland non-glacial streams originate from both H_2CO_3 and H_2SO_4 weathering of carbonate minerals. The second most important contribution of solutes in the inland non-glacial streams is from H_2CO_3 weathering of silicate minerals, while H_2SO_4 weathering of silicate minerals contributes only minor amounts of solutes. In coastal non-glacial streams, the greatest solute contribution is from H_2SO_4 weathering of carbonate minerals and secondarily by H_2SO_4 weathering of silicate mineral. In the coastal non-glacial streams, approximately 10 to 25% of solutes originate from H_2CO_3 weathering of silicate minerals while solute contributions from H_2CO_3 weathering of carbonate minerals are negligible.

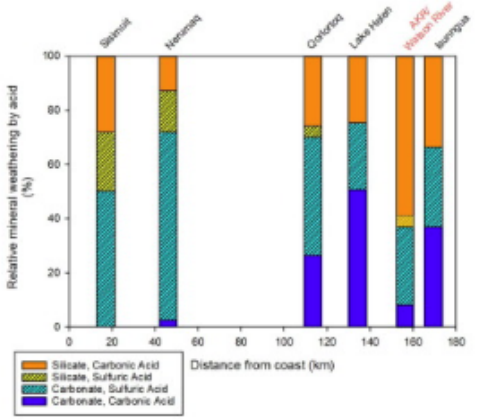

Download : Download high-res image (135KB) Download : Download full-size image

Fig. 4. Calculated average relative abundances of chemical weathering. Weathering is divided by mineral and acid including silicate (warm colors) and carbonate (cool colors) minerals and carbonic acid (plain pattern) and sulfuric acid (hatched pattern). Names of areas are listed above the bars: black text represents non-glacial streams; red text indicates the proglacial streams draining the entire Watson River watershed. (For interpretation of the references to colour in this figure legend, the reader is referred to the web version of this article.)

In AKR/WR, ~65% of the total solutes originate from H_2CO_3 weathering of silicate and carbonate minerals, similar to the fraction of solutes derived from H_2CO_3 weathering in inland deglaciated watersheds (Fig. 4). However, ~60% is derived from silicate minerals with the remaining 5% from carbonate minerals. In contrast, only about 25% of solutes in inland non-glacial streams originate from H_2CO_3 weathering of silicate minerals with 25 to 50% derived from H_2CO_3 weathering of carbonate minerals.

4.3. Sr isotope ratios

Bedload $^{87}Sr/^{86}Sr$ ratios vary less (average = 0.711 ± 0.004 (2 σ)) than dissolved $^{87}Sr/^{86}Sr^*$ ratios in all of the non-glacial and proglacial streams sampled for this study; variation among all dissolved $^{87}Sr/^{86}Sr^*$ ratios is ~0.05 (Fig. 5). The inland watersheds have dissolved $^{87}Sr/^{86}Sr^*$ ratios that are elevated above bedload values (average = 0.739 ± 0.008 (2 σ)) while the coastal deglaciated watersheds have values similar to the bedload values (average = 0.711 ± 0.003 (2 σ)). Qorlortoq samples have the greatest range of dissolved $^{87}Sr/^{86}Sr^*$ ratios of 0.037 (0.71769 to 0.75460) among the non-glacial streams, similar to their large range in specific conductivities (Fig. 2a). The other non-glacial streams have a smaller total range of dissolved $^{87}Sr/^{86}Sr^*$ ratios of <0.007. AKR/WR exhibits a range of ~0.02 (0.72442 to 0.74445) for dissolved $^{87}Sr/^{86}Sr^*$ ratios, which is about half the range observed in all of the non-glacial streams (Fig. 5). However, in contrast with the non-glacial streams, where average $^{87}Sr/^{86}Sr^*$ ratios decrease from the ice toward the coast, the AKR/WR has the lowest dissolved $^{87}Sr/^{86}Sr^*$ ratios near the ice sheet. The values increase toward the sample location a few kilometers downstream of the confluence between the northern and southern tributaries, and then remain approximately constant with distance downstream.

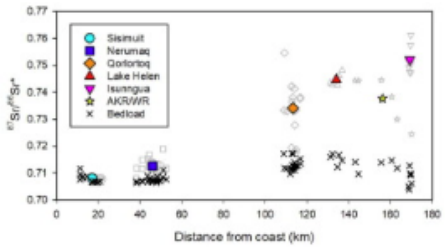

Download : Download high-res image (55KB) Download : Download full-size image

Fig. 5. $^{87}Sr/^{86}Sr^*$ ratios with distance from the coast in non-glacial and proglacial streams. Decreasing offsets between bedload samples (black x's) and aerosol-corrected stream waters reflect increased extent of weathering with moraine age and precipitation. Open symbols are individual samples, filled symbols are averages for each area. Sisimiut, Nerumaq, Qorlortoq, and Lake Helen data are from Scribner et al. (2015). Symbols as in Fig. 2. (For interpretation of colour in this figure, the reader is referred to the web version of this article.)

5. Discussion

5.1. Potential weathering reactions

The decreasing offset between dissolved and bedload Sr isotope ratios in the inland to coastal non-glacial streams (Fig. 5) reflects a reduction in the contribution of ^{87}Sr from chemical weathering (Scribner et al., 2015). A similar pattern of decreasing $^{87}Sr/^{86}Sr$ ratios is observed in glacial streams that drain progressively older weathering surfaces (Blum et al., 1993, Anderson et al., 2000) and in decreasing $^{87}Sr/^{86}Sr$ values of soil leachates combined with relatively constant values for soil digests from glacial chronosequences in the Wind River Mountains of Wyoming (Blum and Erel, 1997). Weathering sources of ^{87}Sr in recently exposed mountain moraines have been attributed to weathering of Rb-rich biotite characterized by highly radiogenic $^{87}Sr/^{86}Sr$ ratios (e.g., Blum et al., 1993, Blum and Erel, 1997, Taylor et al., 2000, Erel et al., 2004, Andrews and Jacobson, 2018). Although we have not determined which specific mineral phases contribute to weathering in the coastal watersheds, the relative proportion of silicate weathering increases toward the coast (Fig. 4). The simultaneous decrease in the offset of $^{87}Sr/^{86}Sr$ ratios between stream water and bedload and the increase in silicate weathering could thus suggest: (1) ^{87}Sr has been preferentially leached from biotite (e.g., Andrews and Jacobson, 2018), (2) the biotite has been preferentially weathered to vermiculite, and/or (3) the dominant weathering mineral switches to silicate phases with $^{87}Sr/^{86}Sr$ ratios lower than those in biotite.
Ionic concentrations of stream water may provide information on which mineral phases are weathering and thus potential sources of ^{87}Sr to the non-glacial streams. Coastal non-glacial streams have K* concentrations that are around 20 times lower compared to Na* concentrations from inland deglaciated watersheds (Electronic Annex, Fig. EA-1). In contrast, bedload of the non-glacial streams have average K/Na molar ratios that vary little between the inland (3.6) and coastal (2.4) deglaciated watersheds (Electronic Annex). The similarity in bedload composition of the non-glacial streams suggests biotite content in the sediment has not decreased appreciably, and thus the trend in

dissolved Sr isotope ratios is most likely due to preferential leaching of ^{87}Sr from biotite (e.g., Erel et al., 2004, Andrews and Jacobson, 2018) and/or a switch to weathering a silicate phase, such as plagioclase, with lower $^{87}Sr/^{86}Sr$ ratios than biotite.
The decrease in K* concentrations relative to Na* concentrations from inland to coastal non-glacial streams suggests increased weathering of less reactive, ^{87}Sr-poor major silicate minerals, such as plagioclase feldspars, toward the coast. This increased plagioclase weathering could reflect production of the stronger acid H_2SO_4 compared to H_2CO_3 in the coastal deglaciated watershed (Fig. 4). Assuming the H_2SO_4 originates from sulfide mineral oxidation (e.g., Torres et al., 2014, Martin, 2017), there appears to be less oxidation of sulfide minerals in inland deglaciated watersheds. Arid inland conditions may limit sulfide mineral oxidation, which would be enhanced in the relatively more humid coastal environments. The resulting production of a strong acid, in addition to the increased exposure age and precipitation, would contribute to the greater weathering maturity in coastal deglaciated watersheds (e.g., Scribner et al., 2015).
With the exception of Qorlortoq, the range of $^{87}Sr/^{86}Sr^*$ ratios of samples collected within individual non-glacial streams is smaller by about half than the range (~0.02) in $^{87}Sr/^{86}Sr^*$ ratios between the AKR northern tributary headwaters and the main channel of AKR (Fig. 5). Although the AKR northern tributary shows this large range, the $^{87}Sr/^{86}Sr^*$ ratios remain constant below the confluence of the AKR northern and southern tributaries (Fig. 6). The variation in $^{87}Sr/^{86}Sr^*$ ratios of AKR samples also corresponds with downstream changes in K*/Na* ratios (Fig. 6), but unlike the non-glacial streams, the decrease in K*/Na* ratio with distance from the ice in the proglacial system is associated with an increase in $^{87}Sr/^{86}Sr^*$ (Fig. 6). Although some in-stream weathering may occur in AKR/WR (e.g., Ryu and Jacobson, 2012), the downstream trends of decreasing K*/Na* and increasing $^{87}Sr/^{86}Sr^*$ ratios suggests other processes may affect solute concentrations and isotope ratios (Andrews and Jacobson, 2018).

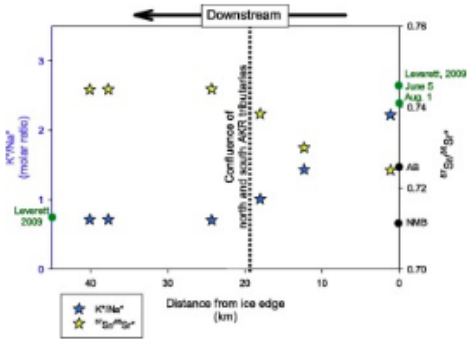

Fig. 6. Downstream variations of K*/Na* (blue stars) and $^{87}Sr/^{86}Sr^*$ ratios (yellow stars) in AKR/WR. Green points on y-axes represent K*/Na* and $^{87}Sr/^{86}Sr^*$ ratios for the Leverett Glacier drainage in samples collected 57 days apart, taken from Hindshaw et al. (2014). The K*/Na* ratio also shifted over the sampling period but the change is smaller than the point. Black points on the right y-axis represent the average $^{87}Sr/^{86}Sr$ ratios of the AB and NMB terrains reported in Colville et al. (2011). The vertical black dotted line represents the confluence of the northern and southern AKR tributaries. (For interpretation of the references to colour in this figure legend, the reader is referred to the web version of this article.)

5.2. AKR/WR compositions from glacial source water mixing and in-stream reactions

Supra- and sub-glacial runoff from the Isunnguata Sermia, Russell, and Leverett glaciers (Fig. 1c) are the dominate water sources to the AKR system because of limited discharge from non-glacial tributaries in the arid region near the ice. Subglacial watersheds extend inland and are underlain by differing lithologies of NMB and AB group rocks, which likely provide distinct solute compositions to the discharging water (Fig. 1c, Lindbäck et al., 2015). The location of the NMB-AB contact under the ice is uncertain, but its northeast-southwest trend in the exposed region (Dawes, 2009) suggests NMB rocks underlie western portions of the Isunnguata Sermia, Point 660, and northwestern portion of the Sandflugtdalen subglacial watersheds, while AB rocks underlie the southeast portion of the Sandflugtdalen subglacial watershed (Pedersen et al., 2013, Lindbäck et al., 2015).

The subglacial sources of water, the rocks that react with subglacial water, and the Sr isotope ratios of those rocks are critical for interpreting the Sr isotope ratios of the AKR/WR system. Sr isotope ratios of bedload sediment where NMB rocks are exposed range between 0.7118 and 0.7123, while bedload sediment from AB rock exposures range between 0.7228 and 0.7254 (Colville et al., 2011, Reyes et al., 2014; Fig. 6). Similar to the NMB values, bedload sediment from AKR/WR averages 0.7117 (total range 0.0085) and suspended sediment from the northern tributary headwaters has an $^{87}Sr/^{86}Sr$ ratio of 0.71184 (Electronic Annex). Suspended sediment Sr isotope ratios increase downstream to an average of 0.7180, with a total range of 0.003. These data suggest bedload sediment of the AKR/WR originates primarily from NMB rocks while the suspended sediment at the headwaters originates from NMB rocks but has increasing contributions from AB rocks downstream. Dissolved $^{87}Sr/^{86}Sr^*$ ratios are higher by 0.012 than the NMB bedload and suspended load sediment at the headwaters of the AKR/WR, while downstream, dissolved $^{87}Sr/^{86}Sr^*$ ratios are higher by 0.018 than AB stream bedload and the suspended load sediment (Fig. 6). Offsets to higher dissolved $^{87}Sr/^{86}Sr^*$ ratios suggests variable amounts of preferential weathering of ^{87}Sr of freshly comminuted sediment from NMB and AB rocks, respectively.

The spatial distribution of $^{87}Sr/^{86}Sr$ ratios of AKR/WR waters and NMB and AB bedload sediments suggests NMB bedrock may influence solutes delivered to the headwaters of the northern tributary, while AB bedrock may influence solutes delivered to the AKR southern tributary. However, dissolved Sr isotope ratios and Sr* concentrations plot above values expected from mixing of putative end-members (Table 4) of AKR northern and southern tributary waters (Fig. 7). This offset could result from changing end-member compositions through time as observed at the Leverett glacier outflow (Hindshaw et al., 2014). However, time variations of end-member composition appears to have a limited role in the offset, considering the change in Leverett end-member composition is far less than the difference between the Isunngua and Leverett end-member compositions. Alternatively, in-stream weathering reactions (e.g., Ryu and Jacobson, 2012), for example in sandur sediment (Deuerling et al., 2018), could alter in-stream compositions and contribute to the offset. Although end-member compositions and in-stream weathering appear to affect AKR/WR water composition, its primary control is from mixing of water from distinct sub-glacial watersheds with different

mineralogical compositions and weathering reactions (e.g., Andrews and Jacobson, 2018).

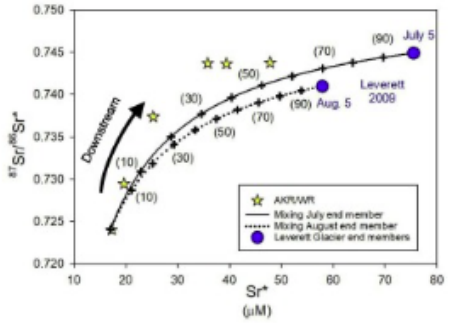

Download : Download high-res image (153KB) Download : Download full-size image

Fig. 7. Cross plot of $^{87}Sr/^{86}Sr^*$ and K^*/Na^* ratios of the AKR/WR with modeled mixing lines using the headwater values from the northern AKR tributary as one end-member and two values from the southern AKR tributary, one collected July 5, 2009 (solid line) and the other collected Aug. 1, 2009 (dotted line) as the second end-member. Numbers in parentheses indicate mixing percentages. Black arrow indicates downstream direction of collected samples (yellow stars). (For interpretation of the references to colour in this figure legend, the reader is referred to the web version of this article.)

5.3. Mass balance estimates of CO_2 weathering sources and sinks

We use the stoichiometry of weathering reactions (Table 3) to estimate relative roles of CO_2 in weathering of proglacial AKR/WR and deglaciated watersheds. This estimate is made by partitioning of CO_2 exchange for each of the weathering reactions shown in Table 3 (Electronic Annex, equations 27 and 28) and summing the change in moles of CO_2 for each reaction after correction for marine aerosol inputs. These reactions include consumption of CO_2 from carbonic acid weathering (reactions 1–3) and production of CO_2 from sulfuric acid weathering of carbonate minerals (reaction 4). Sulfuric acid weathering of silicates (reactions 5 and 6, Table 1) does not impact CO_2; however, these reactions must be considered in the mass balance because they produce cations used in the calculations. Results of the calculations show a wide range in the amount of CO_2 consumed or produced per liter of water during weathering reactions, both between proglacial and non-glacial streams as well as between inland and coastal non-glacial streams (Fig. 8). However, our model results suggest that the difference in CO_2 consumption or production per liter is greater between inland and coastal non-glacial streams than in proglacial streams. Although these relationships likely vary through the melt season as flow conditions change, our observed difference in weathering reactions can be used to evaluate potential differences in these reactions and resulting CO_2 consumption and production between proglacial and non-glacial streams.

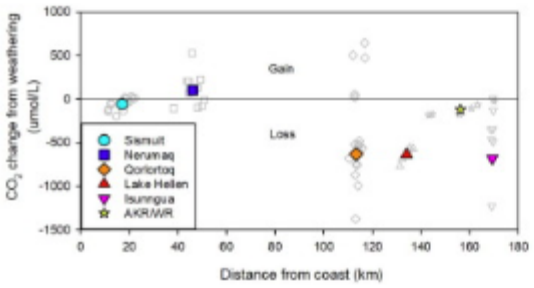

Download : Download high-res image (51KB) Download : Download full-size image

Fig. 8. Calculated loss (negative values) or gain (positive valuates) of CO_2 derived from mineral weathering per liter of water with distance from the coast for non-glacial and proglacial streams. Open symbols are individual samples, filled symbols are average values for each region.

Water emerging from below the Isunnguata Glacier was estimated to have P_{CO2} values supersaturated with respect to atmospheric CO_2 based on mass balance modeling (Ryu and Jacobson, 2012). This modeled supersaturation was proposed to decrease downstream as a result of atmospheric evasion (~25%) and in-stream mineral weathering reactions (~75%). We also estimate that CO_2 weathering consumption increases downstream from ~23 μM CO_2/liter to ~170 μM CO_2/liter in the AKR northern tributary and then remains approximately constant downstream of the confluence of the northern and southern tributaries of AKR (Fig. 8). This change could reflect in-stream weathering although differences in the source water compositions and their weathering regimes as shown by mixing based on Sr isotopes (Fig. 7) may also contribute to the apparent CO_2 consumption. Regardless of the changes in CO_2 consumption within the proglacial stream, per liter weathering sources and sinks of CO_2 vary more in the non-glacial streams than within AKR/WR (Fig. 8). Chemical weathering in inland deglaciated watersheds (Isunngua, Lake Helen, and Qorlortoq) consumes an average of ~580 μmol CO_2/liter. In contrast, weathering in the coastal Sisimiut watersheds consumes on average ~55 μmol CO_2/liter, while weathering in the Nerumaq watershed produces ~100 μmol CO_2/liter. The reduced weathering consumption of CO_2 in the coastal compared to the inland deglaciated watersheds stems from decreased H_2CO_3 weathering as well as production of CO_2 by an increase in the H_2SO_4 weathering of carbonate mineral as weathering matures with exposure age and precipitation (Fig. 4).

In AKR/WR, most weathering (~60%) stems from H_2CO_3 weathering of silicate minerals (Fig. 4). Although this reaction consumes CO_2, the low solute concentrations of the proglacial river results in low amounts of CO_2 consumed per liter relative to inland non-glacial streams (Fig. 8). Arid conditions of the inland deglaciated watersheds limit discharge of non-glacial streams relative to the proglacial AKR/WR and thus total weathering consumption of CO_2 as reflected in compositions of the inland non-glacial streams is likely lower than weathering consumption of CO_2 in the proglacial stream. In contrast, discharge from coastal non-glacial streams is larger than from inland non-glacial streams because of elevated precipitation. In Sisimiut, the weathering consumption of ~55 μmol CO_2/liter is about half the uptake observed in AKR/WR, while

in Nerumaq, weathering generates a source of ~100 μmol CO_2/liter, which approximately matches the per liter weathering sink in AKR/WR. Depending on discharge from these coastal non-glacial rivers, their weathering reactions could modulate CO_2 weathering uptake in proglacial streams. Consequently, weathering sources and sinks of CO_2 should be considered for both proglacial and non-glacial streams in addition to sub-glacial weathering (e.g., Tranter et al., 2002) when estimating changes in CO_2 cycling of glacial forelands during the retreat of continental ice sheets. Furthermore, absolute values, rather than per-volume sources and sinks should be compared, which requires measurements of stream discharge as well as composition.

5.4. Implications for fluxes of weathering products

As the GrIS began to retreat following the Last Glacial Maximum, most runoff would have been through short proglacial streams characterized by immature weathering similar to the extant inland deglaciated and AKR/WR watersheds. This drainage would likely have provided a flush of water with $^{87}Sr/^{86}Sr$ ratios elevated above bedrock values (and presumably radiogenic Pb isotopes, e.g., Foster and Vance, 2006, Kurzweil et al., 2010, Crocket et al., 2012), typical of inland non-glacial and proglacial streams. With continued retreat to its present position, the areal extent of coastal deglaciated watersheds with mature weathering characteristics would have increased relative to deglaciated and proglacial watersheds with immature weathering. Considering the differences in weathering products in inland and coastal non-glacial streams, the retreat of the GrIS should have increased runoff from regions with mature weathering. The increase of weathering maturity suggests weathering would have switched from reactive carbonate minerals to less reactive silicate minerals, H_2SO_4 would become a more prominent weathering acid, CO_2 consumption would decrease, Sr isotopes would stabilized at values similar to the bulk sediment (i.e., less radiogenic) and offsets between dissolved and bedload $^{87}Sr/^{86}Sr$ values (and probably Pb isotopes as well) would have decreased.

The total flux of these reaction products to the ocean will depend on relative discharge from proglacial, as well as inland and coastal non-glacial streams. Our limited discharge data suggest modern coastal non-glacial streams have specific discharge similar to proglacial streams in western Greenland (Table 1), which are likely higher than inland non-glacial streams (Hasholt and Sogaard, 1978) as a result of arid conditions derived from katabatic winds off of the ice sheet. Solute concentrations are greater by several orders of magnitude in coastal non-glacial than proglacial streams (e.g., Fig. 2a), which have similar specific discharges (Table 1). Solutes derived from weathering in coastal deglaciated watersheds may thus have a greater impact on ocean and atmospheric chemistry than weathering in proglacial watersheds. The impact of this effect would depend on the relative contributions from non-glacial and proglacial streams as well as the distribution of “coastal-like” versus “inland-like” deglaciated watersheds. The development of “coastal-like” deglaciated watersheds that are characterized by elevated weathering maturity depends on exposure age (Blum and Erel, 1997, Anderson et al., 2000) as well as relative amounts of precipitation (Scribner et al., 2015). As ice sheets continue to retreat in a warming world, the areal extent of deglaciated watersheds will increase at the expense of proglacial watersheds and the extent of inland deglaciated

watersheds will likely migrate with the ice sheet. Therefore, weathering maturity in coastal deglaciated watersheds could affect marine isotope records, (e.g., Foster and Vance, 2006, Crocket et al., 2012, Basak and Martin, 2013), the weathering control on high latitude stream CO_2 exchange (e.g., Ryu and Jacobson, 2012) (Andrews and Jacobson, 2018) as well as potentially nutrient fluxes (e.g., Hawkings et al., 2016, Hawkings et al., 2017) as Earth's climate warms and ice sheets continue to retreat.

6. Conclusions

Our evaluation of five deglaciated areas and one proglacial stream in the foreland of the GrIS suggests that weathering differs between proglacial and deglaciated watersheds, and to an even greater extent between inland and coastal deglaciated watersheds as exposure increases weathering maturity. Although proglacial streams are known to contribute important solute fluxes to the ocean, our results suggest discharge from non-glacial streams may contribute solutes that differ in magnitude and composition from those delivered by proglacial streams. The major unknown in the global magnitude of these fluxes stems from limited information on water discharge volumes from the watersheds, although preliminary assessments based on available data suggest that the specific discharge from proglacial streams is similar to specific discharge from coastal non-glacial streams. Because non-glacial streams have solute concentrations that can be more than an order of magnitude greater than proglacial streams, their solute delivery may be proportionally higher than previously recognized. Of the solutes evaluated here, weathering maturity appears to control Sr isotope ratios and CO_2 weathering consumption/production, leading to differences between proglacial, coastal and inland non-glacial streams. Consequently, evaluations of changes in these solute fluxes during continental ice sheet retreat should consider evolution of weathering as discharge from coastal non-glacial streams increases relative to discharge from proglacial streams.

Acknowledgements

We thank Daniel Collazo, Cecilia Scribner, Andrea Portier and Mike Davlantes for help with field work, and Ann Heatherington for assistance with isotopic analyses. We also thank the Bureau of Minerals and Petroleum, Government of Greenland for allowing this work to be conducted under Export license 027/2013. Data from the Greenland Ecosystem Monitoring Programme were provided by Asiaq – Greenland Survey, Nuuk, Greenland. We thank Dave Richards and an anonymous reviewer for their thorough reviews that greatly improved the paper. We acknowledge support from the National Science Foundation grants ARC-1203773 and OPP-1603452.

APPENDIX A. SUPPLEMENTARY MATERIAL

Supplementary data to this article can be found online at https://doi.org/10.1016/j.gca.2018.11.025

References

J. Abermann, S.M. Myreng, J. Cristóbal, D. Petersen, M. Olsen**Small rivers in the big picture** Greenland ecosystem monitoring annual report cards, 2017, Arhus University, DCE - Danish Centre for Environment and Energy (2018), pp. 20-22

N.J. Anderson, R. Harriman, D.B. Ryves, S.T. Patrick **Dominant factors controlling variability in the ionic composition of west greenland lakes** Arct. Antarct. Alp. Res., 33 (2001), pp. 418-425

S.P. Anderson, J.I. Drever, C.D. Frost, P. Holden **Chemical weathering in the foreland of a retreating glacier** Geochim. Cosmochim. Acta, 64 (2000), pp. 1173-1189

S.P. Anderson, J.I. Drever, N.F. Humphrey **Chemical weathering in glacial environments** Geology, 25 (1997), pp. 399-402

L.C. Andrews, G.A. Catania, M.J. Hoffman, J.D. Gulley, M.P. Lüthi, C. Ryser, R.L. Hawl ey, T.A. Neumann **Direct observations of evolving subglacial drainage beneath the Greenland Ice Sheet** Nature, 514 (2014), pp. 80-83

M.G. Andrews, A.D. Jacobson **Controls on the solute geochemistry of subglacial discharge from the Russell Glacier, Greenland Ice Sheet determined by radiogenic and stable Sr isotope ratios** Geochim. Cosmochim. Acta (2018)

J. Bamber **Climate change: Shrinking glaciers under scrutiny** Nature advance online publication (2012)

J. Bamber, A. Tedstone, M. King, I. Howat, E. Enderlin, M. van den Broeke, B. Noel **Land ice freshwater budget of the Arctic and North Atlantic Oceans: 1. Data, methods, and results** J. Geophys. Res. Oceans, 123 (2018), pp. 1827-1837

C. Basak, E.E. Martin **Antarctic weathering and carbonate compensation at the Eocene-Oligocene transition** Nat. Geosci., 6 (2013), pp. 121-124

M.P. Bhatia, S.B. Das, K. Longnecker, M.A. Charette, E.B. Kujawinski **Molecular characterization of dissolved organic matter associated with teh Greenland ice sheet** Geochim. Cosmochim. Acta, 74 (2010), pp. 3768-3784

M.P. Bhatia, S.B. Das, L. Xu, M.A. Charette, J.L. Wadham, E.B. Kujawinski **Organic carbon export from the Greenland ice sheet** Geochim. Cosmochim. Acta, 109 (2013), pp. 329-344

M.P. Bhatia, E.B. Kujawinski, S.B. Das, C.F. Breier, P.B. Henderson, M.A. Charette **Greenland meltwater as a significant and potentially bioavailable source of iron to the ocean** Nat. Geosci., 6 (2013), pp. 274-278

J.D. Blum, Y. Erel **Rb-Sr isotope systematics of a granitic soil chronosequence: The importance of biotite weathering** Geochim. Cosmochim. Acta, 61 (1997), pp. 3193-3204

J.D. Blum, Y. Erel, K. Brown **Sr-87/Sr-86 Ratios of Sierra-Nevada stream waters - implications for relative mineral weathering rates** Geochim. Cosmochim. Acta, 57 (1993), pp. 5019-5025

Cappelen J. (2018) Weather observations from Greenland 1958-2017. DMI Report 18-08.

E.J. Colville, A.E. Carlson, B.L. Beard, R.G. Hatfield, J.S. Stoner, A.V. Rayes, D.J. Ullman **Sr-Nd-Pb isotope evidence for ice-sheet presence on southern Greenland during the last interglacial** Science, 333 (2011), pp. 620-623

K.C. Crocket, D. Vance, G.L. Foster, D.A. Richards, M. Tranter **Continental weathering fluxes during the last glacial/interglacial cycle: insights from the marine sedimentary Pb isotope record at Orphan Knoll, NW Atlantic** Quat. Sci. Rev., 38 (2012), pp. 89-99

P.R. Dawes **The bedrock geology under the Inland Ice: the next major challenge for Greenland mapping** Geol. Survey Denmark Greenland Bull., 17 (2009), pp. 57-60

K.M. Deuerling, J.B. Martin, E.E. Martin, C.A. Scribner **Hydrologic exchange and chemical weathering in a proglacial watershed near Kangerlussuaq, west Greenland** J. Hydrol., 556 (2018), pp. 220-232

A. Dyke, V. Prest **Late Wisconsinan and Holocene History of the Laurentide Ice Sheet*** Géographie Phys. Quater., 41 (1987), pp. 237-263

Y. Erel, J.D. Blum, E. Roueff, J. Ganor **Lead and strontium isotopes as monitors of experimental granitoid mineral dissolution** Geochim. Cosmochim. Acta, 68 (2004), pp. 4649-4663

Y. Erel, Y. Harlavan, J.D. Blum **Lead isotope systematics of granitiod weathering** Geochim. Cosmochim. Acta, 58 (1994), pp. 5299-5306

G. Faure **Principles of Isotope Geology** John Wiley & Sons, New York (1986)

A.A.W. Fitzpatrick, A.L. Hubbard, J.E. Box, D.J. Quincey, D. van As, A.P.B. Mikkelsen, S.H. Doyle, C.F. Dow, B. Hasholt, G.A. Jones **A decade (2002–2012) of supraglacial lake volume estimates across Russell Glacier, West Greenland** The Cryosphere, 8 (2014), pp. 107-121

G.L. Foster, D. Vance **Negligible glacial-interglacial variation in continental chemical weathering rates** Nature, 444 (2006), pp. 918-921

A. Galy, C. France-Lanord **Weathering processes in the Ganges-Brahmaputra basin and the riverine alkalinity budget** Chem. Geol., 159 (1999), pp. 31-60

Y. Harlavan, Y. Erel **The release of Pb and REE from granitoids by the dissolution of accessory phases** Geochim. Cosmochim. Acta, 62 (2002), pp. 34-46

Y. Harlavan, Y. Erel, J.D. Blum **Systematic changes in lead isotopic composition with soil age in glacial granitic terrains** Geochim. Cosmochim. Acta, 62 (1998), pp. 33-46

Y. Harlavan, Y. Erel, J.D. Blum **The coupled release of REE and Pb to the soil labile pool with time by weatehring of accessory phases, Wind River Mountains WY** Geochim. Cosmochim. Acta, 73 (2009), pp. 320-336

B. Hasholt, A. Bech Mikkelsen, M. Holtegaard Nielsen, M. Andreas Dahl Larsen **Observations of runoff and sediment and dissolved loads from the Greenland ice sheet at Kangerlussuaq, West Greenland, 2007 to 2010.** Zeitschrift für Geomorphologie, Supplementary Issues, 57 (2013), pp. 3-27

B. Hasholt, H. Sogaard **Et forsog pa en klimatiskhydrologisk regionsinddeling af Holsteinsborg Kommune (Sisimiut)** Geografisk Tidsskrift-Danish J. Geogr., 77 (1978), pp. 72-92

J. Hawkings, J. Wadham, M. Tranter, E. Lawson, A. Sole, T. Cowton, A. Tedstone, I. Ba rtholomew, P. Nienow, D. Chandler **The effect of warming climate on nutrient and solute export from the Greenland Ice Sheet** Geochem. Persp. Let., 1 (2015), pp. 94-104

J. Hawkings, J. Wadham, M. Tranter, J. Telling, E. Bagshaw, A. Beaton, S.L. Simmons, D. Chandler, A. Tedstone, P. Nienow **The Greenland Ice Sheet as a hot spot of phosphorus weathering and export in the Arctic** Glob. Biogeochem Cycle. (2016)

J.R. Hawkings, J.L. Wadham, L.G. Benning, K.R. Hendry, M. Tranter, A. Tedstone, P. N ienow, R. Raiswell **Ice sheets as a missing source of silica to the polar oceans** Nat. Commun., 8 (2017), p. 14198

J.R. Hawkings, J.L. Wadham, M. Tranter, R. Raiswell, L.G. Benning, P.J. Statham, A. T edstone, P. Nienow, K. Lee, J. Telling **Ice sheets as a significant source of highly reactive nanoparticulate iron to the oceans** Nature Commun., 5 (2014)

R.S. Hindshaw, J.R. Rickli, J. Leuthold, J. Wadham, B. Bourdon **Identifying weathering sources and processes in an outlet glacier of the Greenland Ice Sheet using Ca and Sr isotope ratios** Geochim. Cosmochim. Acta, 145 (2014), pp. 50-71

G. Kamenov, M. Perfit, P.A. Mueller, I.R. Jonasson **Controls on magmatism in an island arc environment: study of lavas and sub-arc xenoliths from the Tabar-Lihir-Tanga-Feni island chain, Papua New Guinea** Contrib. Mineral. Petrol., 155 (2008), pp. 635-656, 10.1007/s00410-007-0262-0

F. Kurzweil, M. Gutjahr, D. Vance, L.D. Keigwin **Authigenic Pb istopes from the Laurentian Fan: changes in chemical weathering and patterns of North American freshwater runoff during the last deglaciation** Earth Planet. Sci. Lett., 299 (2010), pp. 458-465

K. Lambeck, T.M. Esat, E.-K. Potter **Links between climate and sealelvels for the past three million years** Nature, 419 (2002), pp. 199-206

L.B. Levy, M.A. Kelly, J.A. Howley, R.A. Virginia **Age of the Ørkendalen moraines, Kangerlussuaq, Greenland: constraints on the extent of the southwestern margin of the Greenland Ice Sheet during the Holocene** Quat. Sci. Rev., 52 (2012), pp. 1-5

K. Lindbäck, R. Pettersson, A.L. Hubbard, S.H. Doyle, D. van As, A.B. Mikkelsen, A.A. Fitzpatrick **Subglacial water drainage and piracy beneath the Greenland Ice Sheet** J. Geophys. Res., 2015 (2015), pp. 7606-7614

J.B. Martin **Carbonate minerals in the global carbon cycle** Chem. Geol., 449 (2017), pp. 58-72

J.B. Martin, E.E. Martin, K.M. Keuerling **Chemical and Isotopic Compositions of Surface and Pore Waters from Western Greenland, 2013** Arctic Data Center (2018)

L. Meire, P. Meire, E. Struyf, D. Krawczyk, K. Arendt, J. Yde, T. Juul Pedersen, M.J. Hopwood, S. Rysgaard, F. Meysman **High export of dissolved silica from the Greenland Ice Sheet** Geophys. Res. Lett., 43 (2016), pp. 9173-9182

S.H. Mernild, B. Hasholt **Observed runoff, jokulhlaups and suspended sediment load from the Greenland ice sheet at Kangerlussuaq, West Greenland, 2007 and 2008** J. Glaciol., 55 (2009), pp. 855-858

S.H. Mernild, G.E. Liston, C.A. Hiemstra, K. Steffen, E. Hanna, J.H. Christensen **Greenland Ice Sheet surface mass-balance modelling and freshwater flux for 2007, and in a 1995–2007 perspective** Hydrol. Process., 23 (2009), pp. 2470-2484

S.H. Mernild, G.E. Liston, K. Steffen, M. van den Broeke, B. Hasholt **Runoff and mass-balance simulations from the Greenland Ice Sheet at Kangerlussuaq (Sondre Stromfjord) in a 30-year perspective, 1979–2008** The Cryosphere (2010), pp. 231-242

K.G. Miller, M.A. Kominz, J.V. Browning, J.D. Wright, G.S. Mountain, M.E. Katz, P.J. Su garman, B.S. Cramer, N. Christie-Blick, S.F. Pekar **The Phanerozoic record of global sea-level change** Science, 310 (2005), pp. 1293-1298

M. Pedersen, W.L. Weng, N. Keulen, T. Kokfelt **A new seamless digital 1: 150,000 scale geological map of Greenland** Geol. Surv. Den. Greenl, 28 (2013), pp. 65-68

A.K. Rennermalm, L.C. Smith, V. Chu, R. Forster, J. Box, B. Hagedorn **Proglacial river stage, discharge, and temperature datasets from the Akuliarusiarsuup Kuua River**

northern tributary, Southwest Greenland, 2008–2011 Earth Syst. Sci. Data, 4 (2012), p. 1

Rennermalm Asa. K., Smith Laurence. C., Chu Vena. W., Moustafa Samiah. E., Pitcher Lincoln., Gleason Colin. (2014). Proglacial river dataset from the Akuliarusiarsuup Kuua River northern tributary, Southwest Greenland, 2008 – 2013, version 2.0. PANGAEA https://doi.org/10.1594/PANGAEA.838812.

A.V. Reyes, A.E. Carlson, B.L. Beard, R.G. Hatfield, J.S. Stoner, K. Winsor, B. Welke, D .J. Ullman **South Greenland ice-sheet collapse during marine isotope stage [thinsp] 11** Nature, 510 (2014), pp. 525-528

J.-S. Ryu, A.D. Jacobson **CO_2 evasion from the Greenland Ice Sheet: A new carbon-climate feedback** Chem. Geol., 320 (2012), pp. 80-95

C. Scribner, E. Martin, J. Martin, K. Deuerling, D. Collazo, A. Marshall **Exposure age and climate controls on weathering in deglaciated watersheds of western Greenland** Geochim. Cosmochim. Acta, 170 (2015), pp. 157-172

J. Spence, K. Telmer **The role of sulfur in chemical weathering and atmospheric CO_2 fluxes: evidence from major ions, $\delta^{13}C_{DIC}$, and $\delta^{34}S_{SO4}$ in rivers of the Canadian Cordillera** Geochim. Cosmochim. Acta, 69 (2005), pp. 5441-5458

H. Stendal, A.A. Garde **Precambrian mineralising events in central West Greenland (66–70 15'N)** Geol. Survey Denmark Greenland Bull., 7 (2005), pp. 61-64

A.P. Stroeven, C. Hättestrand, J. Kleman, J. Heyman, D. Fabel, O. Fredin, B.W. Goodfe llow, J.M. Harbor, J.D. Jansen, L. Olsen **Deglaciation of Fennoscandia** Quat. Sci. Rev., 147 (2016), pp. 91-121

A.S. Taylor, J.D. Blum, A.C. Lasaga, I.N. MacInnis **Kinetics of dissolution and Sr release during biotite and phlogopite weathering** Geochim. Cosmochim. Acta, 64 (2000), pp. 1191-1208

M. Tranter, M.J. Sharp, H.R. Lamb, G.H. Brown, B.P. Hubbard, I.C. Willis **Geochemical weathering at the bed of the Haut Glacier d'Arolla, Switzerland – a new model** Hydrol Process., 16 (2002), pp. 959-993

M.A. Torres, A.J. West, G. Li **Sulphide oxidation and carbonate dissolution as a source of CO_2 over geological timescales** Nature, 507 (2014), pp. 346-349

D. vanAs, A.B. Mikkelsen, M.H. Nielsen, J.E. Box, L.C. Liljedahl, K. Lindbäck, L. Pitcher, B. Hasholt **Hypsometric amplification and routing moderation of Greenland ice sheet meltwater release** The Cryosphere, 11 (2017), p. 1371

D. van As, A. Hubbard, B. Hasholt, A.B. Mikkelsen, M.R. van den Broeke, R.S. Faustol **Large surface meltwater discharge from the Kangerlussuaq sector of the Greenland ice sheet durin gthe record-warm year 2010 explained by detailed**

energy balance observations The Cryosphere, 6 (2012), pp. 199-209, 10.5194/tc-6-199-2012

J.A. vanGool, G.I. Alsop, U.E. Árting, A.A. Garde, C. Knudsen, A.W. Krawiec, S. Mazur, J. Nygaard, S. Piazolo, C.W. Thomas **Precambrian geology of the northern Nagssugtoqidian orogen, West Greenland: mapping in the Kangaatsiaq area** Geol. Greenland Survey Bull., 191 (2002), pp. 13-23

A.F. White, A.E. Blum, M.S. Schulz, T.D. Bullen, J.W. Harden, M.L. Peterson **Chemical weathering rates of a soil chronosequence on granitic alluvium: I. Quantification of mineralogical and surface area changes and calculation of primary silicate reaction rates** Geochim. Cosmochim. Acta, 60 (1996), pp. 2533-2550

J. Wimpenny, K.W. Burton, R.H. James, A. Gannoun, F. Mokadem, S.R. G **The behaviour of magnesium and its isotopes during glacial weathering in an ancient sheild terrain in West Greenland** EPSL, 304 (2011), pp. 260-269

J. Wimpenny, R.H. James, K.W. Burton, A. Gannoun, F. Mokadem, S.R. Gíslason **Glacial effects on weathering processes: New insights from the elemental and lithium isotopic composition of West Greenland rivers** Earth Planet. Sci. Lett., 290 (2010), pp. 427-437

J.C. Yde, N.T. Knudsen, B. Hasholt, A.B. Mikkelsen **Meltwater chemistry and solute export from a Greenland Ice Sheet catchment, Watson River, West Greenland** J. Hydrol., 519 (2014), pp. 2165-2179

J.C. Yde, N. Tvis Knudsen, O.B. Nielsen **Glacier hydrochemistry, solute provenance, and chemical denudation at a surge-type glacier in Kuannersuit Kuussuat, Disko Island, West Greenland** . Hydrol., 300 (2005), pp. 172-187